Soft Matter

Phase Separation and State Oscillation of Active Inertial Particles

Journal:	*Soft Matter*
Manuscript ID	SM-ART-08-2019-001683.R1
Article Type:	Paper
Date Submitted by the Author:	23-Dec-2019
Complete List of Authors:	Dai, Chengyu; University of Michigan, Chemical Engineering Bruss, Isaac; University of Michigan, Chemical Engineering Glotzer, Sharon; University of Michigan, Chemical Engineering

Soft Matter

ARTICLE TYPE

Cite this: DOI: 00.0000/xxxxxxxxxx

Phase Separation and State Oscillation of Active Inertial Particles

Chengyu Dai,[a] Isaac R. Bruss,[b] and Sharon C. Glotzer*[abcd]

Received Date
Accepted Date

DOI: 00.0000/xxxxxxxxxx

Active matter systems are of great interest for their novel out-of-equilibrium collective behavior. Active Brownian particles (ABPs) are known to exhibit clustering and motility-induced phase separation, and there have been many studies revealing this rich behavior in the overdamped limit of Brownian motion, where inertial effects are insignificant. Here we simulate an Active Inertial Particle (AIP) model where we focus on the underdamped, rather than overdamped limit, to study the interplay between particle inertia and collective behavior, such as phase separation. We show that inertia reduces particle motility due to collisions and a longer time delay for particles to regain speed, thereby suppressing phase separation relative to that observed in the overdamped limit. Additionally, we observe interesting oscillatory behavior between a phase separated steady-state and a homogeneous fluid state that results from inertia-induced collective motion within active clusters due to momentum transfer. Such oscillatory behavior has been reported for ABP systems with particle shape anisotropy, where collective motion is mediated by particle shape anisotropy. Furthermore, we confirm that there is no single characteristic frequency for the oscillatory behavior. The power spectral density is a power law in the high frequency domain, with an exponent close to -2.5.

1 Introduction

Active matter systems are intrinsically out of equilibrium, dissipating energy via irreversible dynamics [1–4]. These systems exhibit rich and and at times exotic collective behavior, such as swarming [5–7], giant number fluctuations [8,9] and phase separation [9,10]. Active matter systems abound in biology (for example swimming bacteria or cell suspensions) [11,12], and experiments have demonstrated artificial swimmers made by chemically propelled colloids or Janus particles [13–15]. A particularly successful minimal model for investigating active matter systems is the Active Brownian Particles (ABP) model [9,10,16], composed of self-propelled isotropic particles subjected to Brownian dynamics, with isotropic pairwise interactions that account for volume exclusion via short-ranged repulsion. Motility-induced phase separation, in which nonequilibrium phase separation of the system into coexisting gas and cluster phases occurs if the particle density exceeds a critical threshold, is observed in simulations of ABP [9,10,17]. Theories explaining motility-induced phase separation in the ABP model employ either a coarse-grained model that reflects the interplay between particle diffusion and local density [4,16,17] or kinetic theories balancing the flux between the active fluid phase and cluster phase [10,18].

Most studies of ABP systems focus on the overdamped limit of Brownian Dynamics, where particle inertia is negligible, in order to apply the model to typical biological and colloidal systems. In such systems, with particle sizes on the scale of nanometers to microns, the dominant fluidic drag from the solvent dominates any particle inertial effects, justifying simplification to the overdamped limit. However, recent works have began to explore the novel phase behavior for active systems with macroscopic components where inertia can be important. One such example is that of millimeter-sized self-propelled diodes [19,20]. There are also some recent studies that explore using underdamped Brownian dynamics to model and simulate active matter systems, such as [21–26], and inertia-driven flocking transition was found in extensile active suspensions [27]. In a relevant work, Mandals et al. reported that inertia can produce a self-sustained kinetic temperature gradient as well as suppress phase separation [28]; however, the mechanism of why or how inertia can suppress phase separation was not the focus of that paper and remains, to our knowledge, unknown. Another closely related investigation is a theoretical study of inertial self-propelled hard disks, which studied the collision and scattering mechanism in details and observed an aligned collective motion phase [29], but in their model they assumed implicit alignment (the active force director will gradually align with the velocity) thus unable to be directly compared with ABP systems.

The rapid expanse of the scope of active matter studies calls

[a] Department of Physics, University of Michigan, Ann Arbor, Michigan 48109, United States
[b] Department of Chemical Engineering, University of Michigan, Ann Arbor, Michigan 48109, United States
[c] Biointerfaces Institute, University of Michigan, Ann Arbor, Michigan 48109, United States
[d] Department of Materials Science and Engineering, University of Michigan, Ann Arbor, Michigan 48109, United States
∗ E-mail: sglotzer@umich.edu

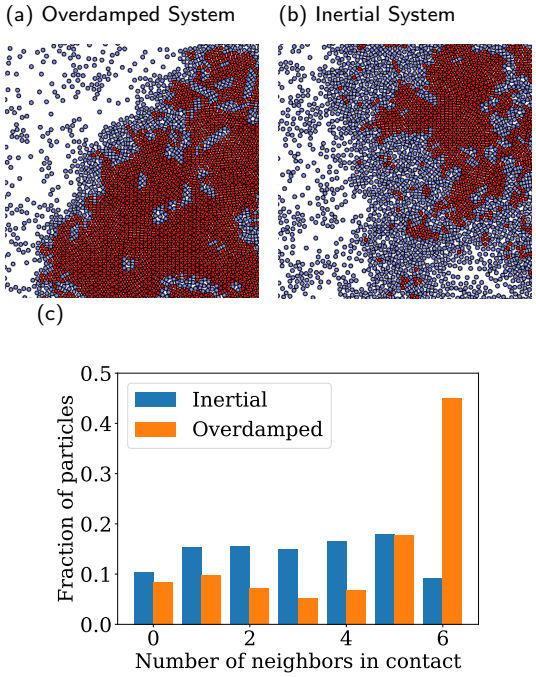

Fig. 1 Due to more elastic collisions, in inertial systems we observe much less well-defined cluster boundaries. Rather, a "transition area" is present between the homogeneous fluid and the active cluster. In the transition area, the local density is high but the hexagonal dense-packed order is absent. (a) A typical active cluster in an overdamped (Brownian) system with $\phi = 50\%$, $F^A\sigma/kT = 100$. (b) A typical active cluster in an inertial system, with $\chi = 1$, $\phi = 50\%$, $F^A\sigma/kT = 100$. In (a, b), particles are colored red if they have six neighbors in contact. (c) Number of contacted neighbors histogram for the (a, b) systems. In the inertial system, the higher fraction of particles with 3-5 contacted neighbors corresponds to the particles in the transition area.

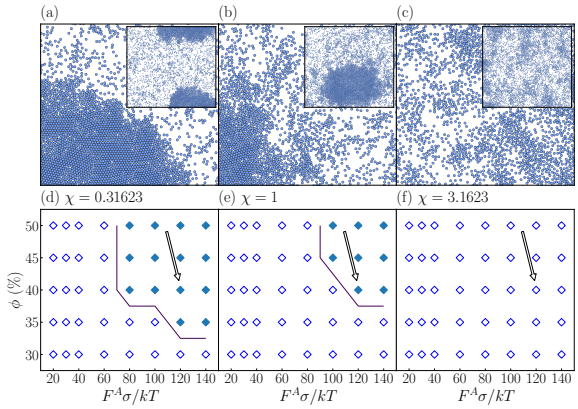

Fig. 2 (a-c): Zoomed simulation snapshot at 300τ for underdamped systems, taken at the statepoints with dimensionless active force $F^A\sigma/kT = 120$, $\phi = 0.4$ and different inertia, each with an inset showing the whole simulation box, $\chi = 0.31623, 1, 3.1623$. (d-e): Cluster fraction as a function of $F^A\sigma/kT$ and ϕ with $\chi = 0.31623, 1, 3.1623$. The arrows show the location of the statepoints of the snapshots in (a-c), while the solid line shows the approximate phase boundary. The solid diamonds represent phase separation and the hollow diamonds represent homogeneous fluid phase.

for a detailed study on the role of particle inertia in the collective phase behavior of self-propelled particles. Moreover, the second-order equations of motion for underdamped Brownian (i.e. Langevin) dynamics offer the flexibility of including an additional timescale in the self-propulsion mechanism (such as chemotaxis, gliding, or twitching), which may have similar effects on the nonequilibrium phase behavior as particle inertia[30]. By using the underdamped equation of motion to model active inertial particle (AIP) dynamics, we aim to contribute to the answer to the open problem posed in[31]: "(Do) activity-induced clustering transitions remain robust when inertial effects are present?" The answer is not immediately obvious. For example, in an AIP system without particle collisions, one might expect particle inertia would simply increase the persistence of a particle's path. However, with particle collisions included, collisions between particles will be more elastic as inertia becomes more significant, and thus after each collision event, an AIP must accelerate to recover its speed, which in turns means a less persistent path.

Here we simulate a 2D system of AIPs interacting as in ABP models with a short-range repulsive potential and subject to a Brownian thermostat with tunable damping. To compare across systems of different damping coefficients, we consider the inertia relative to the active force magnitude. By comparing phase diagrams over a range of dimensionless inertia values, we find that inertia indeed hinders motility-induced phase separation (MIPS). We observe rotating clusters (i.e. cluster-size vortices) as a precursor of cluster instability similar to those found in a 2D experimental Janus system[32] and a simulated ABP system with high Péclet number[33]. Surprisingly, despite the absence of particle shape anisotropy, we also observe density oscillations in AIP systems that resemble oscillatory behavior reported for 2D systems of active shapes, including dumbbells[34], squares[35] and rods[36]. We show that AIP systems can oscillate between phase coexistence and the homogeneous fluid. When examining the power spectral density of the oscillation of the fraction of particles with six neighbors (a proxy for cluster fraction), we find that its high frequency components follow a power law distribution.

2 Model and methods

Active particles were modeled as disks of diameter σ confined to a two dimensional flat surface with periodic boundaries, with positions $\{\boldsymbol{r}_i\}_{i=1}^N$, and self-propulsion directions $\{\theta_i\}_{i=1}^N$. The particles obey Langevin (i.e. completely underdamped Brownian) dynamics via the following equations of motion:

$$m\frac{\partial \boldsymbol{v}_i}{\partial t} = \boldsymbol{F}_i^{ex} + \boldsymbol{F}_i^A - \gamma \boldsymbol{v}_i, \tag{1}$$

$$0 = -\gamma_r \omega_i + \tau_i^R, \tag{2}$$

with the particle label shown as subscript i. Here m is the mass of a particle and $\boldsymbol{v}_i$ and ω_i are the translational and angular velocity, respectively, for the i-th particle. For simplicity, rotational particle inertia was neglected, limiting inertial effects to the translational degrees of freedom. All particles were driven by an active force with the same constant magnitude $\boldsymbol{F}_i^A = F^A\hat{\boldsymbol{v}}_i$. The

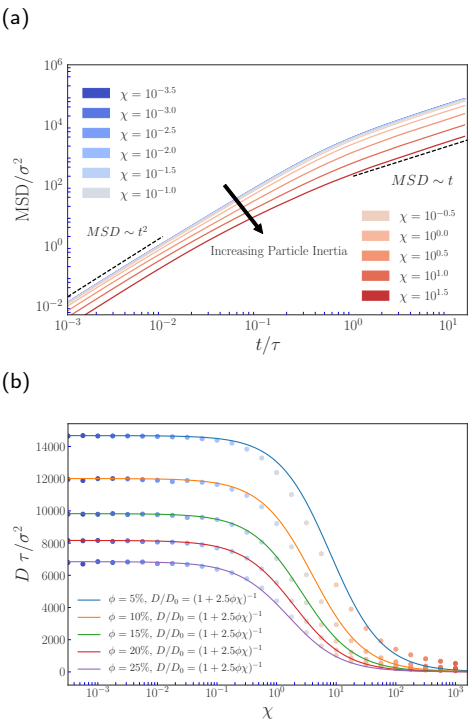

Fig. 3 (a) Mean squared displacement (MSD) versus time for multiple systems with the same $F^A\sigma/kT = 140$ and $\phi = 20\%$, but with various values of dimensionless inertia χ, showing a crossover from ballistic to diffusive behavior. (b) The effective dimensionless diffusion coefficient D decreases significantly with increasing dimensionless inertia χ.

active force director is given by $\hat{\boldsymbol{v}}_i = (\cos\theta_i, \sin\theta_i)$ and follows the equation of motion in Eq. 2. Energy is dissipated through translational and rotational drag, with drag coefficients γ and γ_r, respectively. In the low Reynolds number limit, the translational and rotational drag coefficients are related through the Stokes-Einstein-Debye relations, $\gamma_r = \frac{1}{3}\sigma^2\gamma$[10]. Thermal noise was modeled with a Gaussian random torque $\tau_i^R = \sqrt{2\gamma_r kT}\xi$ with a thermal energy of kT. Here ξ is normalized, zero-mean, white noise. Because the translational noise is usually very small compared to the magnitudes of the active force and interparticle interaction, it was not included in Eq. 1. As in ABP models, we included the volume exclusion force, $\boldsymbol{F}_i^{ex}$, derived from the pairwise WCA potential: $V^{ex} = 4\varepsilon[(\frac{\sigma}{r})^{12} - (\frac{\sigma}{r})^6] + \varepsilon$ for $r < 2^{(1/6)}\sigma$, and $V^{ex} = 0$ otherwise[37].

Simulations were performed on graphic processing units (GPUs) using the HOOMD-blue simulation toolkit[38–40], with data management framework signac[41,42] and data analysis framework Freud[43,44]. N = 10,000 particles were initialized with random nonoverlapping positions and random initial directions for the active force. The natural length scale is the particle diameter σ and time is measured in units of $\tau = \sigma^2\gamma/kT$. In the underdamped (Langevin) case, we adopted a symplectic quaternion integration scheme, NO_SQUISH, to attain better numerical stability[45,46], while for overdamped (Brownian) simulations, a stochastic Euler scheme was applied[47]. In all simulations unless specified otherwise, we used an integration timestep of $2.5 \times 10^{-6}\tau$ and simulations were run for 300τ.

We tracked three important quantities to characterize our simulation systems. The first is the packing fraction, $\phi = N\pi\frac{\sigma^2}{4}/A_{tot}$, which measures the area fraction occupied by particles. The second is the dimensionless force, $F^A\sigma/kT$, which was scaled by adjusting temperature kT while fixing $F^A\sigma/\varepsilon = 24$[4]. This approach ensures that the particles' effective radii during collisions remain the same across a range of active force magnitudes. Note that in the Brownian limit, the dimensionless force $F^A\sigma/kT$ can be interpreted as the Péclet number, as particles accelerate to their terminal velocity within negligible time. In the absence of translational random noise, the physical interpretation of the dimensionless force is the ratio between the rotational persistence timescale and the active timescale, as $F^A\sigma/kT = F^A\sigma/(D_r\gamma_r) = 3\tau_r/(\sigma/\frac{F^A}{\gamma})$ where τ_r is the rotational persistence timescale and $D_r = 1/\tau_r$ is the rotational diffusion constant. The third quantity is dimensionless inertia. By comparing the momentum relaxation time $\tau_m = m/\gamma$ with the time for a particle at its terminal speed to travel its own diameter $\tau_A = \frac{\sigma}{F^A/\gamma}$, the ratio of the two time scales gives the dimensionless inertia $\chi = \tau_m/\tau_A = mF^A/\gamma^2\sigma$. Note that in the related work of Mandal et al.[28], an alternative definition of dimensionless inertia was used by comparing τ_m to the rotational persistence time of the active force director $M = \tau_m/(1/D_r)$ and rotational inertia was considered. When holding M constant, the inertia changes relative to the active force magnitude, which is dominant in active matter systems.

3 Results and Discussion

To gain intuition about inertia's impact on the phase behavior, we first compare two phase separated systems with the ABP and AIP model, in Fig. 1. Due to more elastic collisions, in inertial systems we observe much less well-defined cluster boundaries. Rather, a large "transition area" is present in the AIP systems between the homogeneous fluid and the active cluster. In the transition area, the local density is high but the hexagonal dense-packed order is absent. To avoid confusion, a system is classified as being phase separated if the active clusters can have hexagonal packing persisting over the entire simulation trajectory after its formation.

In Fig. 2(a-c), we show simulation snapshots at the same parameters $F^A\sigma/kT = 120$, $\phi = 0.4$, but with several different values of dimensionless inertia χ. To explore the phase separation behavior, we manually examined each simulation trajectory. Our principle finding is that as inertia increases, the system requires higher $F^A\sigma/kT$ and ϕ to exhibit the same phase separation behavior as shown in Fig. 2(d-f).

To explain the change of the phase behavior, we first investigated how inertia affects particle motility. In the kinetic theory developed by Redner et al.[10], the incoming particle flux from the active fluid to the cluster phase is proportional to the average swimming speed. In AIP systems, inertia reduces a particle's average swimming speed $\langle v \rangle$ from the maximal terminal speed F^A/γ of an overdamped Brownian particle. To isolate the effects of inertia and particle collisions before clustering dominates the dynamics, we focus our attention to the "state points" described by a homogeneous active fluid without phase separation. We evaluate the average mean squared displacement MSD $= \langle \Delta r(t)^2 \rangle$ of

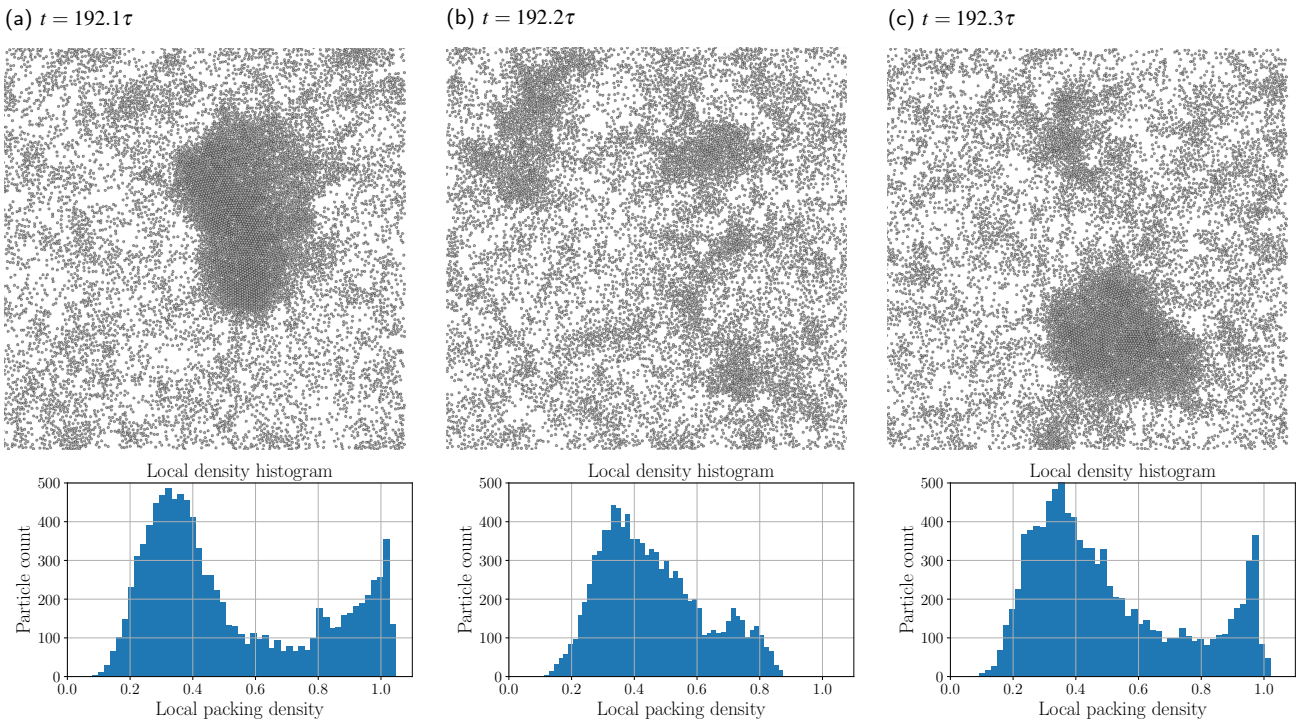

Fig. 4 Snapshots and local density histograms of the same AIP system exhibiting oscillatory behavior at different times. The AIP system is parametrized by $\phi = 40\%$ and $\chi = 3.162$ at the effectively infinite active force limit. In (a-c), simulation snapshots and local density histograms of different timestamps are shown across a cluster disintegration and re-clustering cycle. Note that in (a) and (c) two distinct peaks in local density environments can be observed, with one of the peak corresponding to the dense-packed cluster interior. In (b), the system is in the homogeneous fluid state where only one peak in the local density histogram is observed.

all particles as shown in Fig. 3(a) at a low packing fraction of $\phi = 0.2$ and a constant propulsion force fixed at $F^A\sigma/kT = 140$. On short time scales ($t \ll \tau$), particles behave ballistically with MSD $\sim (v_0 t)^2$, while at long time scales the behavior crosses over to the diffusive regime with MSD $\sim t$, due to the rotational diffusion of the active force director.

At all time scales, systems with larger particle inertia χ have strictly smaller MSD and thus less motility due to collisions, which prevents particles from reaching their maximal terminal speed. This is in contrast to the single particle MSD expression reported in[26], which has no explicit dependence on the particle mass (but has dependence on the moment of inertia of the particle). The interplay between particle collision and inertia is responsible for how inertia changes the MSD reported in Fig. 3. Similarly, for the long time behavior, we observe the generic trend that increasing particle inertia reduces the effective particle diffusion coefficient D. Assuming that a collision event resets a particle's speed to zero, it requires approximately τ_m time to return to its terminal speed. As inertia increases, the time required to accelerate back to terminal speed will increase beyond the free travel time of an active particle, which results in an average speed that may be much lower than the maximal terminal speed. The analytical curve in Fig. 3(b) is $D(\chi) = \frac{D_0}{1+2.5\phi\chi} = \frac{D_0}{1+2.5\phi\tau_m/\tau_A}$, where D_0 is the diffusion constant observed in a system without inertia, i.e. an ABP system. This decrease in D with increasing inertia is consistent with the reduced phase separation shown in Fig. 2.

Surprisingly, our AIP systems also display robust regions of

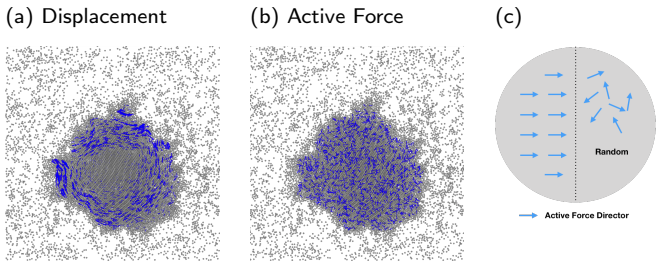

Fig. 5 In the same AIP system as in Fig. 3, at $t = 3.25\tau$, a cluster-size vortex forms in the cluster's dense-packed region. In (a) the blue arrows in the snapshots indicate the orientation and relative magnitude of the displacement field sampled at random positions inside the cluster, while in (b) the active force directors are shown. Despite the isotropic particles and disordered active force directors, particle inertia allows the particles inside clusters to move collectively when experiencing non-zero net forces. (c) To understand why collective motion can form in clusters in AIP systems, consider this constructed active cluster with two halves. The left half have aligned active force directors while the right half is random. With inertia's presence, the cluster would gain net momentum to the right, while in the overdamped (Brownian) limit the cluster would stay still as long as the particles on the edge all have active forces pointing towards the cluster interior to keep it stable. In real AIP systems, the active force directors are not actually aligned but the imbalance of net forces is enough to create cluster-wide collective motion.

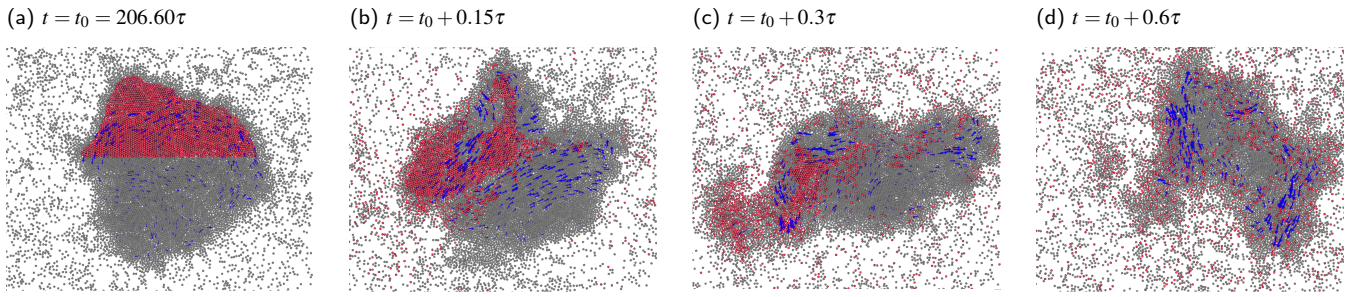

Fig. 6 An example of a (partial) cluster disintegration event in the AIP system's oscillatory state. The AIP system is the same as in Fig. 3. The blue arrows in the snapshots indicate the orientation and relative magnitude of the displacement field, sampled at random positions inside the cluster. The sequence of snapshots demonstrates how collective flow of the cluster's upper section into the low density region causes the cluster to dissolve into a homogeneous fluid phase. The particles that are in the upper section of the cluster at t_0 are colored red in all snapshots. (a) A cluster-size vortex is rotating. (b) The cluster morphed into two parts due to two different directions of collective motion. (c) As the cluster domains flow into a low density region, their density decreases, making the boundary between cluster and homogeneous fluid phase fuzzy. The original cluster domains quickly lose particles and dissolve. (d) After the disintegration event, the particles originally in the upper section are now distributed evenly inside the system.

steady-state oscillation between a homogeneous fluid state and a phase coexistence state. In such oscillatory systems, clusters form from the active fluid and then disintegrate and dissolve back into the active fluid, a phenomenon that is not observed in (overdamped) active Brownian systems. The oscillatory behavior can be easily seen from the two qualitatively different types of local density histograms at different times, shown in Fig. 4. The local density histogram is a unimodal bell-shaped curve in a homogeneous fluid state shown in Fig. 4(b), and has two distinct peaks in phase coexistence shown in Fig. 4(a, c), corresponding to close-packed density inside clusters and lower density in the homogeneous fluid. Note that local packing density can be slightly over 1 due to the internal stress inside the clusters (that is, the non-infinite repulsion force between two particles).

The oscillatory behavior of these AIP systems shows many qualitative similarities with systems of active Brownian squares, in which all of the oscillations observed can also persist over for a very long time ($> 300\tau$) without signs of stopping[35]. Like the Brownian active squares, AIP systems also display cluster-sized vortices that rotate clusters or parts of clusters as a whole, see Fig. 5. The rotating clusters can also be found in experiments of a 2D induced-charge electrophoretic self-propelled Janus colloids system, which sees "interrupted phase separation" due to the rotational collective motion within the largest cluster[32]. In the experimental Janus system, alignment occurs in both the particle displacements and active directors, while in AIP systems only the displacement field is aligned as demonstrated in Fig. 5. Instead of melting from the surface, the collective movements of particles in these vortices induce the cluster disintegration events. Clusters disintegrate and dissolve by large domains collectively flowing into a low density region. However, such disintegration usually happens to parts of the cluster in a multi-step fashion rather than dissolving an entire cluster at once. We occasionally observed very complex flow fields inside dense clusters when multiple cluster domains flow into different regions and dissolve at the same time. An example of such a disintegration event is shown in Fig. 6. To intuitively understand the distinction between clusters in AIP and ABP system, consider an active cluster with two halves, each with different active force directors (Fig. 5(c)), the left half aligned and the right in random directions. In the overdamped limit, such a cluster would stay still, while in AIP systems, such a cluster will gain net momentum. Inertia enables the cluster-wide collective motion.

Despite the similarities in vortex behaviors, AIP systems are unique in that the particles are isotropic. Oscillatory behavior is usually found in active anisotropic particles such as dumbbells[34], squares[35] and rods[36]. Our findings suggest that particle shape anisotropy is not essential to either the formation of global vortices inside active clusters or oscillatory behavior. Rather, what is needed is some memory mechanism to enable the development of collective motion inside the cluster. In active Brownian square systems, particle shape sterically induces particles inside the cluster to effectively interlock with neighboring particles, enabling the cluster to accumulate nonzero torques, which then lead to collective motion in the form of global vortices. In the AIP systems, instead of aligning the particle orientation within a cluster, the momentum transfer that occurs during the collision of cluster domains results in particles either accelerating or scattering in a different direction, forming similar rotating vortices.

We are able to generate time series statistics covering many cluster formation and disintegration cycles by running simulations at 40% density, $\chi = 3.162$ and $F^A\sigma/kT = 5000$ (effectively infinite) at a very high time resolution where each snapshot is separated by $\Delta t = 1/2500\tau$ for a total duration of 100τ. The time series statistics of particle fractions with different numbers of direct contact neighbors are shown in Fig. 7(a-b). In particular, the fraction of particles with 6 neighbors $p_6(t)$, a proxy for cluster fraction, is shown in Fig. 7(a), and oscillates between 0 and 0.25. The time autocorrelation function (ACF) of $p_6(t)$ is shown in Fig. 7(c). By calculating the power spectral density of $p_6(t)$ in Fig. 7(d), we confirm the open conjecture made by Prymidis et al in[35] that the oscillations are not associated with a single characteristic frequency. Interestingly, the high frequency components of the power spectral density (PSD) exhibit a power law distribution in frequencies with exponent between -2 and -3, which is estimated by regression to be approximately $\beta = -2.5$. As shown in the supplementary information, we are still able to observe the steady-state oscillation in simulations with increased system sizes

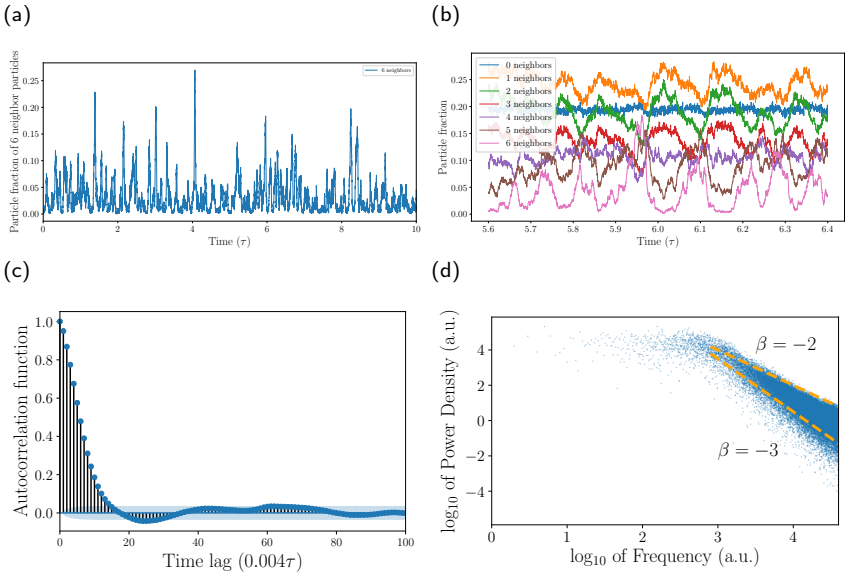

Fig. 7 Time series of the particle fractions with different neighbors in contact. The AIP system is in oscillatory state, with a packing fraction of 40% and $\chi = 3.162$. (a) shows the complete time evolution of particle fraction with 6 neighbors in contact, i.e. particles in dense-packed clusters. (b) shows the magnified version of (a) with higher temporal resolution. The conversion between particle local environments can be clearly seen. (c) shows the autocorrelation function (ACF) for the time series in (a), showing that the correlation time is no longer than 0.1τ in the systems we studied. The blue shade show the 95% confidence band calculated from Bartlett's formula for each lag[48]. Correlation values larger than the magnitude of the blue shade can be considered significant. (d) shows the power spectral density (PSD) for the same time series as (a), with both axes in log scale. The high frequency components of the oscillation between different steady-state behavior appear to follow a power law distribution with exponent between -2 and -3. The exponent was determined by linear regression to be approximately -2.5.

of up to 99,856 particles (316×316 as compared to 100×100 in Fig. 7), which proves that the observed oscillation is not a simulation artifact due to finite system sizes.

4 Conclusion and Future Outlooks

In summary, we have shown that increasing particle inertia discourages clustering and phase separation because particle motility is reduced by the interplay between particle inertia and collisions. We showed that when particle inertia becomes comparable to the magnitude of the active force, phase separation becomes significantly harder. Our findings are relevant to a wide range of self-propelled active systems where particle inertia is non-negligible. One example is a system of mm-sized, vibrated polar disks[49], where, based on our findings, we should expect phase separation to be a rare occurrence. Our findings also demonstrate that coupling between active force orientation and particle environment (mediated by shape anisotropy) is not essential to the formation of active vortices or steady-state oscillation. The coupling between AIP velocities and their local environment suffices to generate interesting non-equilibrium collective behaviors such as oscillations between a homogeneous fluid phase and a phase-separated (clustered) phase and we characterized them by standard time series analysis techniques. Our work demonstrates the important role of particle inertia on the collective behavior of active systems, and we hope it motivates increased attention to the role of inertia in active matter.

We thank Dr. Thi Vo, Dr. Joshua Anderson, Dr. Jens Glaser and Mr. Mayank Agrawal for helpful discussions. This work was supported by the Center for Bio-Inspired Energy Science (CBES), an Energy Frontier Research Center funded by the U.S. Department of Energy, Office of Science, Basic Energy Sciences under Award # DE-SC0000989. Our computational resources are supported by Advanced Research Computing (ARC-Flux) at the University of Michigan, Ann Arbor.

Notes and references

1 A. Baskaran and M. C. Marchetti, *Physical Review Letters*, 2008, **101**, 268101.
2 S. Mishra, A. Baskaran and M. C. Marchetti, *Physical Review E*, 2010, **81**, 061916.
3 M. Marchetti, J. Joanny, S. Ramaswamy, T. Liverpool, J. Prost, M. Rao and R. A. Simha, *Reviews of Modern Physics*, 2013, **85**, 1143.
4 J. Stenhammar, D. Marenduzzo, R. J. Allen and M. E. Cates, *Soft Matter*, 2014, **10**, 1489–1499.
5 T. Vicsek, A. Czirók, E. Ben-Jacob, I. Cohen and O. Shochet, *Physical Review Letters*, 1995, **75**, 1226.
6 J. Toner and Y. Tu, *Physical Review Letters*, 1995, **75**, 4326.
7 J. Toner and Y. Tu, *Physical Review E*, 1998, **58**, 4828.
8 V. Narayan, S. Ramaswamy and N. Menon, *Science*, 2007, **317**, 105–108.
9 Y. Fily and M. C. Marchetti, *Physical Review Letters*, 2012, **108**, 235702.
10 G. S. Redner, M. F. Hagan and A. Baskaran, *Physical Review Letters*, 2013, **110**, 055701.
11 A. Baskaran and M. C. Marchetti, *Proceedings of the National Academy of Sciences*, 2009, **106**, 15567–15572.

12 M. Cates and J. Tailleur, *EPL (Europhysics Letters)*, 2013, **101**, 20010.

13 I. Buttinoni, G. Volpe, F. Kümmel, G. Volpe and C. Bechinger, *Journal of Physics: Condensed Matter*, 2012, **24**, 284129.

14 J. Palacci, S. Sacanna, A. P. Steinberg, D. J. Pine and P. M. Chaikin, *Science*, 2013, **339**, 936–940.

15 I. Buttinoni, J. Bialké, F. Kümmel, H. Löwen, C. Bechinger and T. Speck, *Physical Review Letters*, 2013, **110**, 238301.

16 J. Stenhammar, A. Tiribocchi, R. J. Allen, D. Marenduzzo and M. E. Cates, *Physical Review Letters*, 2013, **111**, 145702.

17 M. E. Cates and J. Tailleur, *Annual Review of Condensed Matter Physics*, 2015, **6**, 219–244.

18 G. S. Redner, A. Baskaran and M. F. Hagan, *Physical Review E*, 2013, **88**, 012305.

19 S. T. Chang, V. N. Paunov, D. N. Petsev and O. D. Velev, *Nature Materials*, 2007, **6**, 235.

20 R. Sharma and O. D. Velev, *Advanced Functional Materials*, 2015, **25**, 5512–5519.

21 K. H. Nagai, Y. Sumino, R. Montagne, I. S. Aranson and H. Chaté, *Physical Review Letters*, 2015, **114**, 168001.

22 B.-Q. Ai and F.-G. Li, *Soft Matter*, 2017, **13**, 2536–2542.

23 A. Manacorda and A. Puglisi, *Physical Review Letters*, 2017, **119**, 208003.

24 B. M. Mognetti, A. Šarić, S. Angioletti-Uberti, A. Cacciuto, C. Valeriani and D. Frenkel, *Physical Review Letters*, 2013, **111**, 245702.

25 Y. Fily, Y. Kafri, A. P. Solon, J. Tailleur and A. Turner, *Journal of Physics A: Mathematical and Theoretical*, 2017, **51**, 044003.

26 C. Scholz, S. Jahanshahi, A. Ldov and H. Löwen, *Nature Communications*, 2018, **9**, 5156.

27 R. Chatterjee, N. Rana, R. A. Simha, P. Perlekar and S. Ramaswamy, *arXiv preprint arXiv:1907.03492*, 2019.

28 S. Mandal, B. Liebchen and H. Löwen, *arXiv preprint arXiv:1902.06116*, 2019.

29 K.-D. N. T. Lam, M. Schindler and O. Dauchot, *New Journal of Physics*, 2015, **17**, 113056.

30 P. Romanczuk, M. Bär, W. Ebeling, B. Lindner and L. Schimansky-Geier, *The European Physical Journal Special Topics*, 2012, **202**, 1–162.

31 C. Bechinger, R. Di Leonardo, H. Löwen, C. Reichhardt, G. Volpe and G. Volpe, *Reviews of Modern Physics*, 2016, **88**, 045006.

32 M. N. van der Linden, L. C. Alexander, D. G. A. L. Aarts and O. Dauchot, *Physical Review Letters*, 2019, **123**, 098001.

33 P. Nie, J. Chattoraj, A. Piscitelli, P. Doyle, R. Ni and M. P. Ciamarra, *arXiv preprint arXiv:1904.07084*, 2019.

34 A. Suma, G. Gonnella, D. Marenduzzo and E. Orlandini, *EPL (Europhysics Letters)*, 2014, **108**, 56004.

35 V. Prymidis, S. Samin and L. Filion, *Soft Matter*, 2016, **12**, 4309–4317.

36 S. Weitz, A. Deutsch and F. Peruani, *Physical Review E*, 2015, **92**, 012322.

37 J. D. Weeks, D. Chandler and H. C. Andersen, *Journal of Chemical Physics*, 1971, **54**, 5237–5247.

38 http://codeblue.umich.edu/hoomd-blue, HOOMD-blue.

39 J. A. Anderson, C. D. Lorenz and A. Travesset, *Journal of Computational Physics*, 2008, **227**, 5342–5359.

40 J. Glaser, T. D. Nguyen, J. A. Anderson, P. Liu, F. Spiga, J. A. Millan, D. C. Morse and S. C. Glotzer, *Computer Physics Communications*, 2015, **192**, 97–107.

41 C. S. Adorf, P. M. Dodd, V. Ramasubramani and S. C. Glotzer, *Computational Materials Science*, 2018, **146**, 220–229.

42 C. S. Adorf, V. Ramasubramani, B. D. Dice, M. M. Henry, P. M. Dodd and S. C. Glotzer, *glotzerlab/signac*, 2019, `https://doi.org/10.5281/zenodo.2581327`.

43 V. Ramasubramani, B. D. Dice, E. S. Harper, M. P. Spellings, J. A. Anderson and S. C. Glotzer, *freud: A Software Suite for High Throughput Analysis of Particle Simulation Data*, 2019.

44 E. S. Harper, M. Spellings, J. Anderson and S. C. Glotzer, *harperic/freud: Zenodo DOI release (Verson 1.2.2)*, 2016, `https://doi.org/10.5281/zenodo.166564`.

45 T. Miller Iii, M. Eleftheriou, P. Pattnaik, A. Ndirango, D. Newns and G. Martyna, *The Journal of Chemical Physics*, 2002, **116**, 8649–8659.

46 H. Kamberaj, R. Low and M. Neal, *Journal of Chemical Physics*, 2005, **122**, 224114.

47 I. Snook, *The Langevin and generalised Langevin approach to the dynamics of atomic, polymeric and colloidal systems*, Elsevier, 2006.

48 P. J. Brockwell, R. A. Davis and M. V. Calder, *Introduction to time series and forecasting*, Springer, 2002, vol. 2.

49 J. Deseigne, O. Dauchot and H. Chaté, *Physical Review Letters*, 2010, **105**, 098001.